EXPERIMENTAL AND NUMERICAL INVESTIGATION ON THE DYNAMIC STABILITY OF A BLUNTED BODY CONFIGURATION

Thomas Gawehn[1], Bodo Reimann[1], Lars Tysell[2], Davide Bonetti[3], Adam Jirasek[2], Emma Johnstone[4], Etienne Clopeau[5], Ali Gülhan[1], Luca Ferracina[6], Rafael Molina[6]

1: German Aerospace Center (DLR), Institute of Aerodynamics and Flow Technology, 51147 Köln / 38108 Braunschweig, Germany
2: FOI, Swedish Defence Research Agency, 164 40 Kista, Sweden
3: Deimos Space UK Ltd., Didcot, Oxfordshire OX11 0QG, United Kingdom
4: Fluid Gravity Engineering Ltd., Emsworth, Hampshire, PO10 7DX, United Kingdom
5: Airbus Defence and Space (SAS), EADS ASTRIUM, 78133 Les Mureaux CEDEX, France
6: European Space and Technology Centre (ESTEC), Flight Vehicles and Aerothermodynamics Engineering Section, 2200 AG Noordwijk ZH, The Netherland

ABSTRACT

The aero shape of ESA's Intermediate eXperimental Vehicle (IXV) is prone to suffer from stability problems in the transonic regime. The actual study aims to avoid the supersonic descent system used for IXV by improving aerodynamic stability with minor modification of the Outer Mold Line (OML). It should be achieved to pass the transonic flight regime at angle of incidence reduced to below 40° and to improve static stability conditions in subsonic with a lift-to-drag ratio higher than 1.

The OML modification is defined within a numerical pre-study. Then, two new configurations are investigated experimentally and numerically to determine static and dynamic aerodynamic coefficients between Mach 0.5 and 2.0. An AErodynamic Data Base (AEDB) is built to analyse the flight performance of the new configurations on a potential re-entry mission. It seems as if the introduced OML modifications are successful to overcome the transonic stability issues of IXV.

Index Terms — Blunt body aerodynamics, static and dynamic stability, IXV aero shape

1. INTRODUCTION

During the atmospheric entry or re-entry of flight vehicles one of the critical issues is the dynamic stability of the vehicle in the transonic regime. This transition phase between supersonic and subsonic flight is known to be particularly hazardous for lifting hypersonic vehicles, whose design is heavily influenced by the need to withstand the harsh environment during hypersonic entry.

In view of the recent experience at ESA on the IXV aero shape and its successful flight, it has been selected as baseline for the future concept Space Rider. But former studies revealed that the IXV configuration has a dynamically instable behaviour in certain flight regimes. In particular, significant transonic static instability at $0° - 40°$ angle of incidence has been confirmed during the IXV project activities and also in the frame of the DERIVAS study where experiments and simulations were performed to assess the aerodynamic behaviour of the IXV configuration [1, 2].

One option for improving the dynamic stability of a vehicle is changing its external shape slightly e.g. by adding small fins. Such modifications could improve static and dynamic stability behaviour and decrease the angle of incidence and thereby increase lift-to-drag ratio. This modification should improve flying qualities of the vehicle in the critical transonic regime and avoid the implementation of supersonic descent systems.

Aim of the present study is to develop a shape modification with help of experimental and numerical tools that enables passing the transonic flight regime at an angle of incidence below 40°, increased stability margin with respect to IXV and achieve a lift-to-drag ratio in subsonic of higher than 1. Further, a static and dynamic aerodynamic data base should be built and the flying qualities of the new configuration be analysed.

2. GEOMETRY DEFINITION PROCESS

First step of the geometry definition process was the analysis of historical finned body concepts. Based on the outcome of the study, two fin types based on different NACA profiles and also different root-to-tip chord length are further analysed. Thereby, position, orientation and inclination angle of the fins are varied systematically.

The FOI EDGE code is a node-centred, edge based finite volume method that solves the Reynolds-Averaged Navier-Stokes compressible equations. Here, it is used to estimate the static aerodynamic coefficients of each of the new finned configurations at flight conditions in the Mach

range $0.6 \leq Ma \leq 1.1$ and angle of incidence range $10° \leq \alpha \leq 30°$. Most of the calculations are performed applying the Spalart-Allmaras turbulence model. A side slip angle of $\beta = 1°$ is set to allow for analysing the static lateral stability, too. Calculations are performed on the flight configuration with flap deflection angles of $\delta_f = 0°$ and $\pm 5°$. The reference parameters are $L_{ref} = 4.4\,m$ and $S_{ref} = 7.26\,m^2$. The Moment Reference Centre (MRC) is set equal to that of IXV: $x_{MRC} = 0.58\,L_{ref}$, $y_{MRC} = 0$ and $z_{MRC} = -0.025\,L_{ref}$.

Within an iterative process, including analysis of simulation results, re-design of the geometry and re-start of the simulation, it is intended to achieve a configuration that is optimized in trans- and subsonic to the prerequisites and stability criteria named in Table 1.

Prerequisites:

Trim angle	$\alpha_{trim} < 30°$
Lift-to-Drag ratio at trim point	$L/D > 1$
Vehicle fit into Vega fairing (like IXV)	

Stability criteria:		**Definition:**
Pitch stability:	$C_{m\alpha} < 0$	$C_{m\alpha} = \frac{\partial C_m}{\partial \alpha}$
Yaw stability:	$C_{n\beta} > 0$	$C_{n\beta} = \frac{\partial C_n}{\partial \beta}$
Roll stability:	$C_{l\beta} < 0$	$C_{l\beta} = \frac{\partial C_l}{\partial \beta}$
Generalized side stability:	$C_{n\beta^*} > 0$	$C_{n\beta^*} = C_{n\beta}\cos\alpha - \left(\frac{I_Z}{I_X}\right) C_{l\beta}\sin\alpha$

Table 1: Prerequisites and stability criteria.

Numerous simulations have been performed and finally a configuration with a NACA $63-015$ profile with its root leading edge at $x = 3.072\,m$, $y = 0.9\,m$ and $z = 0.1\,m$ (from reference point at the nose) is chosen for further investigation. This configuration, named "Dynast_n" is aerodynamically optimized, as far as possible. Based on this shape, a geometrically simplified and easier to manufacture, rectangular shaped fin is developed, named "Dynast_r". It is shown in Figure 1, together with the definition of the aerodynamic coordinate system in the MRC.

Comparison of the numerical simulations for these two configurations revealed, that the aerodynamic performance of the rectangular version seems to be comparable to that with the NACA profile. Therefore, the rectangular version is declared as baseline for the following investigations, but experimental analysis is performed with both configurations, nonetheless.

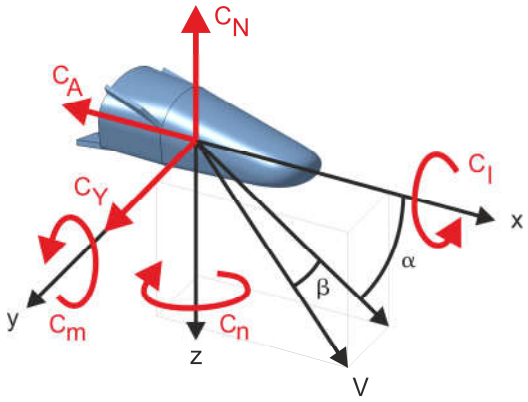

Figure 1: Dynast_r and aerodynamic coordinate system.

3. STATIC SIMULATION RESULTS

Static simulations have been performed for many different configurations, but only selected results of the simulation for configuration Dynast_r are presented hereafter. Primarily, the pitching moment coefficient C_m at four different Mach numbers is shown in Figure 2, plotted against the angle of incidence α. Thereby, the results of the performed simulations (symbols) are connected with straight lines. Solid lines represent the pitching moment for a flap deflection of $\delta_f = 0°$, dashed lines for $\delta_f = +5°$ and long dashed for $\delta_f = -5°$.

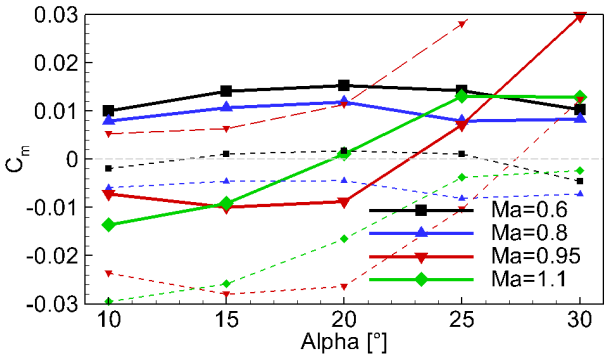

Figure 2: Simulated pitching moment coefficient C_m of Dynast_r, $\delta_f = 0°$ (solid), $\delta_f = +5°$ (dashed) and $\delta_f = -5°$ (long dashed).

From the viewgraph, the static stability conditions for Dynast_r can be estimated: At $Ma = 0.6$ (black) a statically stable trim point ($C_m = 0$ and $C_{m\alpha} < 0$) can be reached for $25° \leq \alpha \leq 30°$ with a flap deflection of $\delta_f \leq +5°$. Also at $Ma = 0.8$ (blue), a stable trim condition is predicted in the range $20° \leq \alpha \leq 30°$ with a flap deflection of $\delta_f \leq +4°$.

Near the sonic barrier, the situation is different. At $Ma = 0.95$ (red), the gradient $C_{m\alpha}$ is positive above $\alpha \approx 15°$, but due to the step width of the calculation of 5°

the magnitude in the range of $20° \leq \alpha \leq 25°$ can only be estimated. Possibly, for small negative flap deflection an instable trim point exists around $\alpha \approx 23°$, but with the gradient small enough to be compensated by the Guidance, Navigation & Control (GNC) system during flight.

At supersonic condition of $Ma = 1.1$ (green), it is assumed that a statically stable trim condition could be found in the range of $25° \leq \alpha \leq 30°$, according to the simulation. Thereby, the flap deflection would be around $\delta_f \approx +4°$. By that, the first prerequisite to achieve a trim angle of $\alpha_{trim} < 30°$ seems to be fulfilled by the Dynast_r configuration, as well as the pitch stability criteria except for $Ma = 0.95$.

As second prerequisite, a lift-to-drag ratio of $L/D > 1$ is demanded for trim conditions. Figure 3 shows the L/D ratio calculated from the simulation results for a flap deflection angle of $\delta_f = 0°$, whereby the flap deflection has only minor influence on the values. As can be seen, for all subsonic conditions, the ratio is higher than 1 at trim conditions and even reaches a value of $L/D \approx 1.4$ at $Ma = 0.6$. Actually for $Ma = 1.1$, a lift-to-drag ratio of more than 1 is achieved at the trim point. Thereby, this prerequisite is also fulfilled by the Dynast_r configuration.

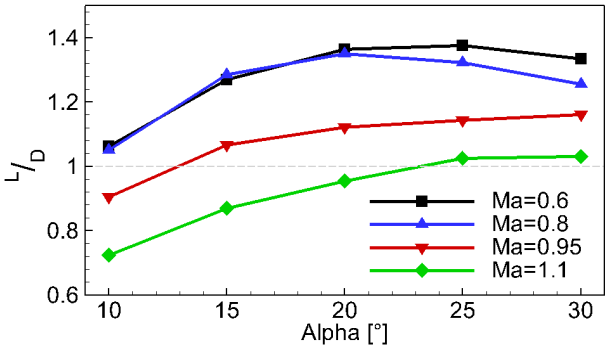

Figure 3: Simulated lift-to-drag ratio L/D of Dynast_r, δ_f =0°.

Concerning the lateral stability criteria, yaw stability ($C_{n\beta} > 0$) is not achieved, but the simulated values are very small. Roll stability criteria ($C_{l\beta} < 0$) is fulfilled and also the generalized side stability criteria ($C_{n\beta^*} > 0$) where the calculated values are plotted in Figure 4. Visibly, the values are positive at trim conditions for all simulated Mach numbers.

To conclude, in the Mach range $0.6 \leq Ma \leq 1.1$ the aerodynamic performance of the newly defined configuration Dynast_r proves to be promising. Therefore, further analysis, including experiments on static and dynamic stability as well as unsteady simulations will be performed with this configuration as the baseline. As far as possible, the configuration with NACA profile will also be investigated, but only results of the Dynast_r configuration will be shown herein.

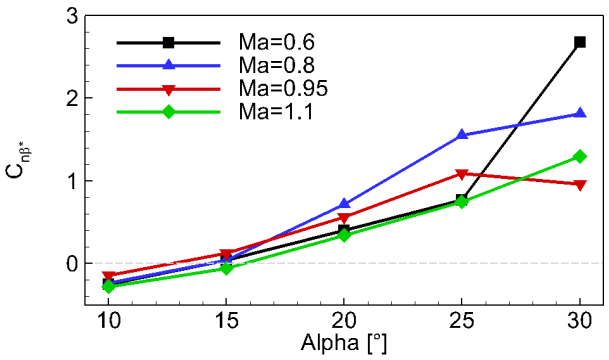

Figure 4: Simulated generalized side stability $C_{n\beta^*}$ of Dynast_r, $\delta_f = 0°$.

4. EXPERIMENTAL INVESTIGATION ON STATIC AND DYNAMIC STABILITY

Wind tunnel tests are performed in the trisonic wind tunnel TMK of DLR Köln which covers a Mach range of $0.5 \leq Ma \leq 5.6$. In supersonic, the flow conditions are set via the stagnation conditions and the area ratio of the flexible nozzle. For transonic investigations, a test section with perforated side walls is used and the flow conditions are set via the adaptable diffuser system downstream.

Two different wind tunnel models are manufactured. One allows for the determination of aerodynamic coefficients with help of an internal 6-component strain gauge balance. The other model is equipped with a cross-flexure enabling only pitch motion positioned in a way that the model's centre of rotation equals the defined MRC. The second model allows for the determination of dynamic derivatives using the free oscillation technique. Both models have exchangeable sets of flaps and also an exchangeable fin section to allow for tests with rectangular or NACA-shaped fins or, for reference purposes, with the finless IXV configuration.

Details on the facility, the model design and the measurement techniques are presented in [3].

4.1. Static aerodynamic tests

Table 2 gives an overview on the static aerodynamic tests with all three configurations (Dynast_r, Dynast_n and IXV) in the Mach range $0.5 \leq Ma \leq 2.0$. Most tests with the finned configurations are performed with a flap deflection angle of $\delta_f = 0°$ or $+5°$, whereby tests on the reference configuration IXV are only performed with $\delta_f = 0°$. At all tests in the supersonic test section ($Ma \geq 1.3$), large Quartz glass windows allow for a visualization of density gradients in the flow field by means of a schlieren optical setup. In the transonic test section ($Ma \leq 1.1$), due to the perforated side walls, simultaneous flow visualization is not possible.

			Dynast_r			Dynast_n			IXV
	Mach	$Re_{\infty L}$ (10^6)	δ_f=-5°	0°	+5°	δ_f=-5°	0°	+5°	0°
Transonic tests	0.5	1.6		X	X		X	X	
	0.6	2.0		X	X		X	X	X
	0.7	2.3-2.4					X	X	
	0.8	2.7-2.8		X	X		X	X	X
	0.85	3.0					X		
	0.9	3.2-3.5		X	X		X	X	
	0.95	3.6-3.7	X	X	X	X	X	X	X
	1.05	4.5-4.8		X	X		X	X	
	1.1	5.0-5.1		X	X		X	X	X
Supersonic tests	1.3	4.1-4.2		X	X		X	X	X
	1.4	4.1-4.5	X	X	X	X	X	X	X
	1.5	4.0-4.3		X	X		X	X	X
	1.8	4.2-4.6		X	X		X	X	X
	2.0	4.3-4.7		X	X		X	X	X

Table 2: Test matrix of static aerodynamic tests.

For a static test, the model is aligned at low angle of incidence at wind tunnel start up. After the flow condition is stabilized, the angle of incidence is altered continuously up and down and the aerodynamic forces and moments are recorded in an α-range of $-2° \leq \alpha \leq 35°$ (transonic tests) and $-2° \leq \alpha \leq 44°$ (supersonic tests). Then, the tunnel is shut down again. All data are recorded with an acquisition rate of 100 Hz and stored directly on disk. The coefficients are calculated after the test with an in house tool.

4.2. Static coefficients

The effect of the fins can be experienced best by comparing the pitching moment coefficient C_m of Dynast_r with that of the reference configuration IXV. In Figure 5, this comparison is plotted for $Ma = 0.6$ and 0.95 (upper chart) as well as for Ma=1.1 and 1.5 (lower chart). Thereby, the solid lines represent the measured data for Dynast_r and the dashed lines those for IXV.

While IXV shows a statically instable behaviour at $Ma = 0.6$ for the complete investigated α-range, the gradient of $C_{m\alpha}$ is about zero around $\alpha \approx 20°$ for Dynast_r and even negative for higher angle of incidence. In combination with a positive flap deflection, this would allow for a statically stable trim condition at $Ma = 0.6$ in the range $20° \leq \alpha \leq 30°$. Higher angles of incidence should be avoided as unsteady effects seem to occur beyond $\alpha \approx 32°$.

$Ma = 0.95$ proves again to be a difficult condition with respect to static stability. Although, static stability could not be fully achieved by implementation of the fins, Dynast_r provides lower values for C_m and a gradient $C_{m\alpha}$ that is significantly decreased, at least for angels of incidence below $\alpha \approx 22°$, in comparison to IXV. However, both configurations possess a discontinuity on the C_m slope at $\alpha \approx 28°$. It is assumed that this is caused by the onset of flow separation on the leeward side of the vehicle, but could not be proved within the experimental test campaign.

At supersonic conditions (Figure 5, lower chart), statically stable trim points can be found for IXV and Dynast_r with $\delta_f = 0°$, but with fins, the trim angle is about 2° lower at $Ma = 1.1$ and about 6° lower at $Ma = 1.5$. This reduction in trim angle directly affects the performance of the configuration at trim condition with respect to the L/D ratio that is plotted in Figure 6.

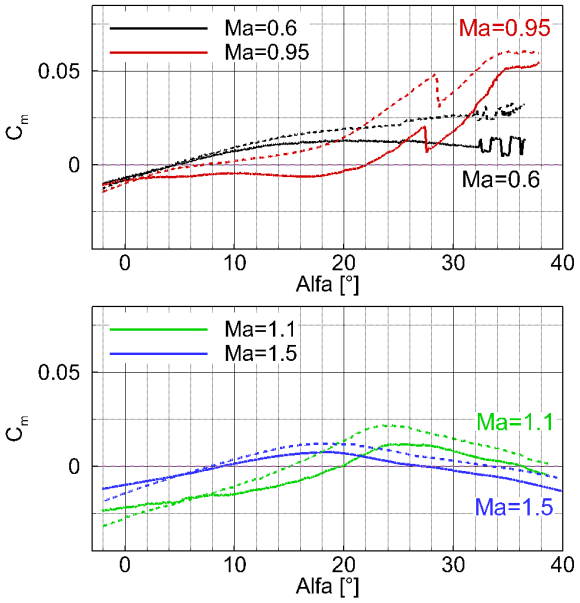

Figure 5: Pitching moment coefficient C_m of Dynast_r, $\delta_f = 0°$ (solid) and IXV, $\delta_f = 0°$ (dashed).

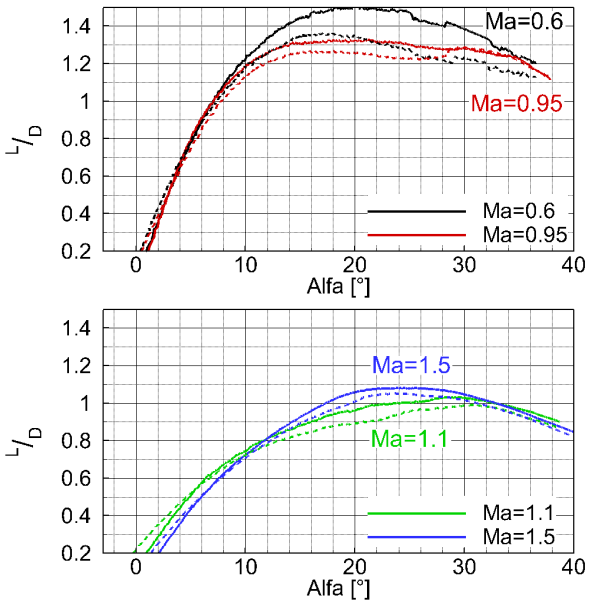

Figure 6: Lift over Drag ratio L/D of Dynast_r, $\delta_f = 0°$ (solid) and IXV, $\delta_f = 0°$ (dashed).

Comparison of Dynast_r (solid lines) with the reference configuration IXV (dashed lines) reveals that implementation of the fins itself already increases the L/D ratio at all plotted Mach numbers. Additionally, the reduction in trim angle further increases the L/D ratio at trim condition for Dynast_r. The maximum value, achieved at $Ma = 0.6$ is $L/D \approx 1.5$. This is even higher than the predicted value at that Mach number from numerical simulation during the geometry definition phase (Figure 3).

So far, the numerically predicted behaviour of the Dynast_r configuration has been proved by the experimental results. It showed that static longitudinal performance could be improved with respect to the IXV configuration. Lateral stability has been investigated numerically and will not be researched experimentally at this point. Instead, the next steps are focused on the analysis of the longitudinal dynamic behaviour of the new configuration.

4.3. Dynamic tests

The free oscillation technique has been chosen to determine dynamic derivatives for the Dynast configurations experimentally. Within such a test, the sting angle is set prior to wind tunnel start up. The cross-flexure is blocked until the test conditions are set. Then the model is deflected and released several times using an implemented mechanism. Wind tunnel data and the oscillation of the model measured via the instrumented cross-flexure are recorded with a frequency of 4 kHz. Then, cross-flexure is blocked again and the wind tunnel shut down.

As these tests could only be performed around the trim point where the resulting pitching moment is about zero, suitable trim conditions for each Mach number have to be found in a first step. Using the static aerodynamic coefficients, the trim points are determined by interpolating linearly the pitching moment data recorded with different flap deflections $\delta_f = 0°$ and $\pm 5°$.

As for supersonic conditions, a trim point is already found with $\delta_f = 0°$ (Figure 5, lower chart) the dynamic tests are performed at these conditions. If a minor offset of the pitching moment from zero remains during the test, this can be easily compensated for the next test by a slight shift in incidence angle. Only for reference purposes, some tests are performed with different flap deflection and thus at different trim angle.

In transonic and subsonic, the pitching moment slope is nearly horizontal around the potential trim condition (Figure 5, upper chart) and the curve shifted in first approximation up and down by alteration of the flap deflection angle δ_f. Nonetheless, dynamic tests using the free oscillation technique are possible at indifferent or even slightly instable static trim conditions due to the resetting moment of the cross-flexure. Thereby, trim condition cannot be achieved by alteration of the angle of incidence, but only by adaptation of the flap deflection angle δ_f. This led to the manufacturing of 10 sets of flaps between $\delta_f = 0°$ and $+5.5°$.

Figure 7 shows in blue the processed cross-flexure signal for one release of the Dynast_r model at $Ma = 2.0$ and $\alpha_{trim} = 37.2°$. From these data, using the ansatz of a harmonic oscillation, the signal is reconstructed (red). By that, the angular frequency ω and the damping δ of the oscillation can be determined. Then, with the cross-flexure characteristics known from calibration, the aerodynamic stiffness $C_{m\alpha}$ and pitch damping sum $(C_{mq} + C_{m\dot{\alpha}})$ can be calculated. Due to the chosen setup, the components of the pitch damping sum cannot be determined separately.

Details on the free oscillation technique are given in [3].

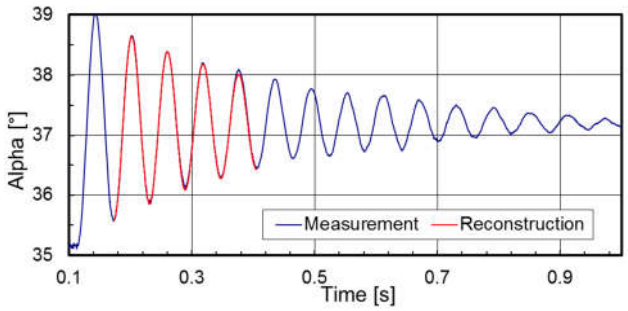

Figure 7: Recorded model oscillation (blue) and reconstructed signal (red), $Ma = 2.0, \delta_f = 0°, \alpha_{trim} = 37.2°$.

Dynamic tests are only performed for both Dynast configurations. Tests with the reference configuration IXV would only have been possible at supersonic conditions. These conditions proved to be less critical and were therefor not elaborately investigated.

As one major result of the dynamic investigation, the pitch damping sum $(C_{mq} + C_{m\dot{\alpha}})$ for Dynast_r is presented in Figure 8 for trim conditions in the Mach range $0.5 \leq Ma \leq 2.0$. Tests could not be performed at $Ma = 0.95$. The upper and lower margin has been calculated from the uncertainties of all test parameters applying the error approximation law of Gauss.

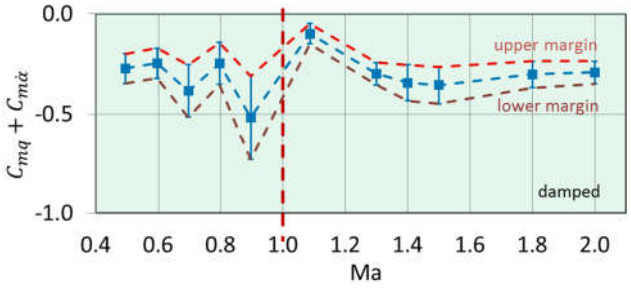

Figure 8: $(C_{mq} + C_{m\dot{\alpha}})$ of Dynast_r configuration.

The pitch damping sum is negative in the complete Mach range. In combination with $C_{m\alpha} < 0$ this gives **static and dynamic stability** of the Dynast_r configuration at the corresponding test conditions, i.e. for $Ma \geq 1.1$.

At statically indifferent or instable conditions, i.e. for example at $Ma = 0.6$, the negative pitch damping sum leads to slower dynamics for the transition of the vehicle to a stable point making the system simpler to control. Positive derivatives in contrast would lead to a system that is stiffer to control and may result in an oversized GNC system.

5. NUMERICAL SIMULATION ON STATIC AND DYNAMIC STABILITY

Two different approaches for numerical determination of dynamic derivatives are applied:

1. Simulation of a free oscillation using the DLR TAU code and
2. Simulation of a forced oscillation using the FOI EDGE code.

The TAU code is a finite volume method that solves steady and unsteady Euler and Navier-Stokes equations developed by DLR. In the present case, a flight mechanics and structure mechanics coupling and the overlapping grid technique are applied. Details on the code, the computational domain and the performed simulations are presented in [4].

The EDGE code developed by FOI has already been used within the geometry definition phase and is briefly described in section 2. At this project phase, steady and unsteady simulations are performed using a combination of a Reynolds Averaged Navier Stokes simulation near the surface and a Large Eddy Simulation in the far field. This type of simulation is called: hybrid RANS/LES simulation and is applied together with a grid deformation and interpolation technique. For further information on the computational domain and the simulation results see [5].

In both cases, primarily, numerous steady-state simulations at different angles of incidence are performed to determine numerical trim conditions and to achieve a suitable starting solution for the dynamic simulation. As the computational effort in the whole is rather comprehensive, only three test cases are simulated and the results compared to the experiments:

1. Supersonic: $Ma = 2.0, \delta_f = 0°$,
2. Transonic: $Ma = 1.1, \delta_f = 3.5°$ and
3. Subsonic: $Ma = 0.5, \delta_f = 3.5°$.

5.1. Steady-state simulations

Especially at supersonic conditions, schlieren images from experiment can be compared to the density gradients calculated from numerical simulations. As the experimental line-of-sight method integrates along the optical path, an in-house tool is applied to calculate synthetic schlieren images from the simulated density fields.

In the wind tunnel, a Z-arrangement is used to record schlieren on a monochromatic Prosilica $GE4000$ camera (frame rate: up to $5\,Hz$, min. exp. time: $140\,\mu s$, sensor: CCD, res.: $4008x2672\,px$, bit depth: $16\,bit$). Due to the perforated side walls in the transonic test section, schlieren images are only recorded at Mach numbers $Ma \geq 1.3$.

Exemplarily, Figure 9 shows on top a schlieren image of a static wind tunnel test at $Ma = 2.0$ ($\delta_f = 0°$) with the model at $\alpha = 40°$ angle of incidence. Below, the synthetic schlieren image calculated from a steady-state TAU simulation applying the Spalart Allmaras turbulence model is plotted. Obviously, the basic flow structures of experimental and numerical image coincide fairly well although the flow separation on the leeward side of the model is only poorly recognizable in the printed version of the experimental image. Shock interaction with the sting downstream of the model's base is also visible in both cases.

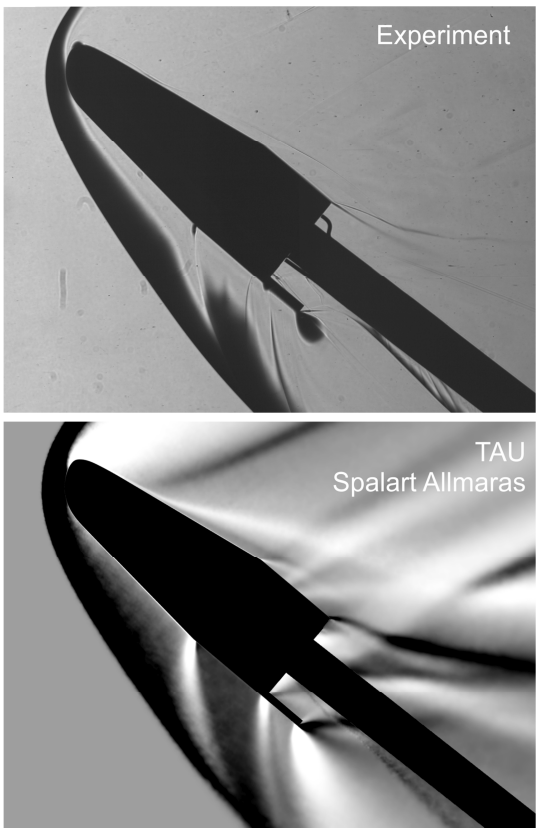

Figure 9: Experimental and numerical schlieren images of Dynast_r at $Ma = 2.0, \delta_f = 0°, \alpha \approx 40°$.

5.2. Unsteady simulations

Simulation of a free oscillation with DLR TAU code

Starting point of the unsteady simulation is a model orientation deflected by $\Delta\theta = +1.5°$ from the numerically determined trim angle. A steady state flow solution at that

incidence angle is used as the initial restart solution. Then, unsteady flow (URANS) simulations with full coupling of rigid body motion (1-Degree-of-Freedom - only pitch) are performed. Thereby, only the vehicle is free to oscillate around the centre of rotation while the sting is fixed in space. Overlapping grid technique is used.

Figure 10 shows the simulated motion at $Ma = 2.0$ ($\delta_f = 0°$) of the model (TAU w/o spring) in green together with the corresponding wind tunnel experiment in grey (TMK #025). Obviously, the resulting frequency of the simulated oscillation is much lower and the numerical trim condition ($\alpha_{trim,sim} = 36.5°$) alters slightly from the experimental one ($\alpha_{trim,exp} = 37.2°$). Therefore, a second unsteady simulation is performed that takes the mechanical moment of the cross-flexure into account. The resulting oscillation is plotted in blue (TAU with spring). The trim condition is not changed, but this time, the oscillation frequency is comparable to that of the wind tunnel experiment. Thus, simulations with and without cross-flexure are performed for all three test cases.

Determination of the derivatives from the calculated oscillation data is performed equally to the treatment of the experimental results. As expected, the simulations with and w/o cross-flexure lead to nearly equal dynamic coefficients. Results for the other test cases as well as details on the simulation and analysis procedure referring to the free oscillation simulation can be found in [4].

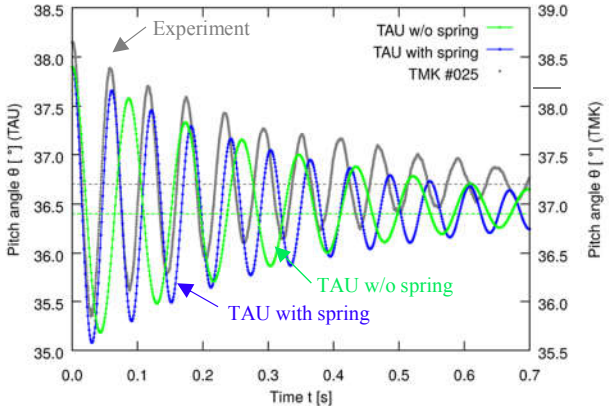

Figure 10: Simulated oscillation of Dynast_r, Ma=2.0, δ_f=0°, $\alpha_{trim,sim}$=36.5°, $\alpha_{trim,exp}$=37.2°.

Simulation of a prescribed motion with FOI EDGE code

Dynamic simulations are performed around the calculated static trim points with the oscillation frequencies taken from the corresponding TAU simulations as external parameters. The grid around the vehicle is deformed to $\theta_{min} = -1.5°$ and $\theta_{max} = +1.5°$, whereas the sting is fixed. In between these two positions the grid is computed by interpolation. In order to reduce the computational time the number of inner iterations is set to 30, thus sacrificing convergence.

The unsteady simulation for $Ma = 2.0$ around $\alpha_{trim} = 39.4°$ covers 3.87 cycles. The calculated pitching moment C_m is plotted against the deflection angle θ in Figure 11. Thereby, the original data shown in grey are relatively noisy. Before being further analysed, the data are smoothed and averaged. This leads to the anti-clockwise oriented curve printed in blue that surrounds the green area. Then, the pitch damping sum is calculated by solving a closed-loop integral on C_m.

For details on simulation procedure, results and the calculation of the dynamic coefficients, please refer to [5].

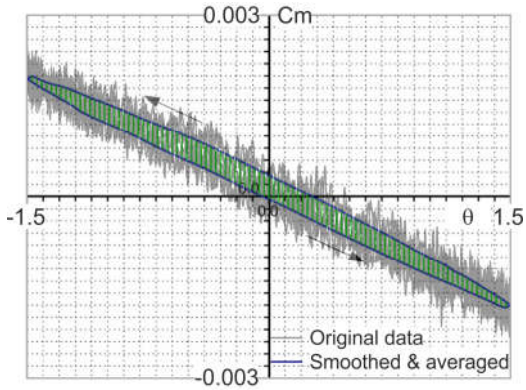

Figure 11: Simulated pitching moment C_m against deflection angle θ for Dynast_r, $Ma = 2.0, \delta_f = 0°, \alpha_{trim} = 39.4°, \omega = 103.6\ s^{-1}$

6. DISCUSSION OF EXPERIMENTAL AND NUMERICAL RESULTS

Conformity of dynamic experimental and numerical results can be evaluated by comparing the following parameters:

- Trim angle α_{trim}
- Angular oscillation frequency ω
- Pitching moment damping derivative $(C_{mq} + C_{m\dot{\alpha}})$
- Pitching moment slope $C_{m\alpha}$

The parameters are listed in Table 3. As no trim condition was found in the EDGE simulation at $Ma = 1.1$, but the prescribed motion was nonetheless simulated, the corresponding trim angle is set in brackets.

	Ma	α_{trim} (°)	ω (1/s)	$C_{mq} + C_{m\dot{\alpha}}$	$C_{m\alpha}$ (1/°)
TMK exp.	2.0	37.2	107.7	-0.292	-1.26E-03
	1.1	30.2	77.8	-0.099	-1.16E-04
	0.5	26.6	72.3	-0.272	-3.71E-04
TAU with CF	2.0	36.4	103.3	-0.282	-1.08E-03
	1.1	37.4	79.8	-0.366	-1.90E-04
	0.5	33.6	78.9	-0.182	-1.49E-03
EDGE RANS/LES	2.0	39.4	103.6	-0.297	-1.25E-03
	1.1	*(38.0)*	*83.0*	*-0.255*	*-4.71E-04*
	0.5	34.0	78.6	-0.210	-8.66E-04

Table 3: Comparison of experimental and numerical dynamic results.

At $Ma = 2.0$, the determined experimental and numerical results differ in an acceptable manner. At transonic ($Ma = 1.1$) or subsonic condition ($Ma = 0.5$), the deviation is higher which could be caused by the difference in trim angle. But, in the whole, experiment and both simulations lead to negative values for aerodynamic stiffness $C_{m\alpha}$ and aerodynamic damping $\left(C_{mq} + C_{m\dot{\alpha}}\right)$ and thus to a statically and dynamically stable vehicle behaviour at the investigated test conditions.

7. FLYING QUALITIES ANALYSIS

AErodynamic Data Bases (AEDBs) are built for both Dynast configurations (Dynast_r and Dynast_n). They include the experimental results of static and dynamic tests in the Mach range $0.5 \leq Ma \leq 2.0$ as well as the calculated uncertainties of the derived data. Thereby, the data sets are restricted to the longitudinal motion of the vehicle.

The data bases are used to analyse the flying qualities of both configurations with respect to two potential entry trajectories provided by ESA. Based on this analysis, two different trim strategies are developed (Figure 12): One aims to minimize the work load on the GNC system and the other to stay "optimum in the entry corridor".

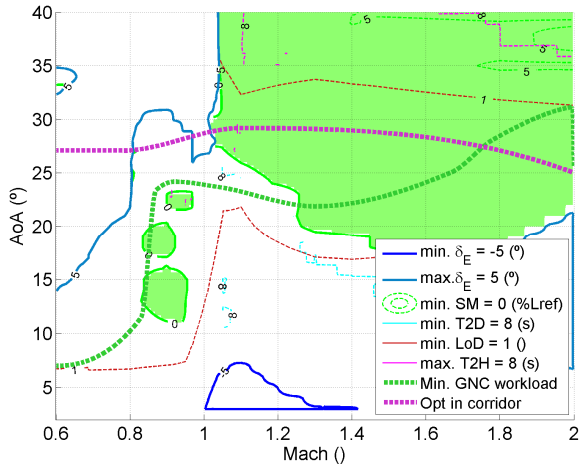

Figure 12: Proposed trim strategies for Dynast_r, green: Min. GNC workload, purple: Opt. in corridor.

The analysis carried out has brought to light the following recommendations:

- The aerodynamic data bases should be completed in longitudinal and extended to lateral directional plane to perform full 6-DoF trajectory simulations.
- A fine tuning of the CoG of the vehicle is recommended, in order to achieve positive static margin throughout a wider part of the entry corridor.
- A comparison of the aerodynamic behaviour of the two finned configurations with one finless configuration (IXV/Space Rider) could help in justification between the options.
- The elevator deflection limits considerably (saturation) the feasibility of the entry corridors. Therefore investigation on wider elevator deflections is recommended.
- The flying qualities analysis were limited to nominal conditions (no dispersions on MCI or AEDB) while a robust trim line design will require the introduction of dispersions and a statistical assessment of the flying qualities performance.
- A consistent aerodynamic separation was found, which affects in particular the pitching moment coefficient. The complete picture, in the 6 components, would be highly recommended, as it would allow investigating lateral directional stability, in particular in transonic, and the effectiveness of the finned configurations.

For further details of the flight performance analysis see [6].

8. CONCLUSION

The IXV aero shape was modified by implementing small fins to improve static stability conditions in trans- and subsonic. The aerodynamic performance of two new configurations was investigated. The flying qualities analyses proved to be promising in decreasing the trim angle and thereby increasing the L/D ratio. In the investigated Mach number range, the new configurations proved to be either statically stable, indifferent or only slightly instable. Dynamically, damped oscillations were recorded for transonic and subsonic test conditions. Though, the modified aero shapes seem to overcome the stability issues of IXV in the transonic range. Nevertheless, in order to achieve a deeper understanding of the configuration capabilities and performance it is suggested to perform additional investigations taking into account the recommendations from the flying qualities analysis.

9. REFERENCES

[1] Gülhan, A.; Klevanski, J.; Gawehn, T.; *Experimental study on the dynamic stability of the IXV configuration*. 8th European Symposium on Aerothermodynamics for Space Vehicles, Lisbon, Portugal, March 2-6, 2015.

[2] Reimann, B.; *Numerical Prediction of Longitudinal Dynamic Stability for a Lifting Body in Transonic Flow*. 34th AIAA Applied Aerodynamics Conference, Washington, D.C., USA, 13-17 June, 2016, AIAA2016-3578.

[3] Gawehn, T.; Gülhan, A.; *Experimental study on static and dynamic stability of a blunt body configuration*. FAR conference, Monopoli, Italy, 30 September - 3 October, 2019.

[4] Reimann, B.; Gawehn, T.; *Numerical Investigation of Wind Tunnel Test to Measure Dynamic Stability*. FAR conference, Monopoli, Italy, 30 September - 3 October, 2019.

[5] Tysell, L.; Dalenbring, M.; *Hybrid RANS/LES computations of pitch damping derivatives for a blunt body configuration*. FAR conference, Monopoli, Italy, 30 September - 3 October, 2019.

[6] Bonetti, D.; Medici, G.; Arnao, G. B.; Riley, D.; *Flying Qualities Analysis Of Dynast (Dynamic Stability Of Capsules And Blunt Bodies At Angle Of Attack)*. FAR conference, Monopoli, Italy, 30 September - 3 October, 2019.